Forecasting circulation in the Cilician Basin of the Levantine Sea

E. Özsoy, A. Sözer

Ocean Sci. Discuss., 3, 1481–1514, 2006
www.ocean-sci-discuss.net/3/1481/2006/

Papers published in *Ocean Science Discussions* are under
open-access review for the journal *Ocean Science*

Forecasting circulation in the Cilician Basin of the Levantine Sea

E. Özsoy and A. Sözer

Institute Marine Sciences, Middle East Technical University, Erdemli-Mersin, Turkey

Received: 31 May 2006 – Accepted: 21 June 2006 – Published: 11 September 2006

Correspondence to: E. Özsoy (ozsoy@ims.metu.edu.tr)

Abstract

The Cilician Basin/Shelf Model is adapted for studying the shelf circulation in the Cilician Basin – Gulf of İskenderun region of the Levantine Basin of the Eastern Mediterranean between the Turkish Mediterranean coast, Syria and the island of Cyprus. The model initial conditions and open boundary conditions are supplied by the ALERMO regional model of the Levantine Sea, while interactive surface flux boundary conditions are specified by an atmospheric boundary layer sub-model using calculated water properties and surface atmospheric variables supplied by the Skiron atmospheric model, within the nested modelling approach of the MFSTEP (Mediterranean Forecasting System: Towards Environmental Predictions) project. Sensitivity tests are performed for alternative surface boundary conditions. Model performance for shelf/mesoscale forecasts is demonstrated.

1 Introduction

The Cilician Basin coastal system occupies the northeastern part of the Eastern Mediterranean Levantine Basin between Cyprus and Turkey, and includes the wide, shallow continental shelf areas of Mersin and İskenderun Bays (Fig. 1). The continental shelf adjoining Mersin and İskenderun Bays is one of the widest in the entire Levantine Sea (excluding the Nile Cone) where the coastal bathymetry is often very steep. Taurus and Amanos mountain ranges bound the Cilician Basin respectively in the north and east, lined with narrow "riviera" coastal plains except in the vast delta plains of the Seyhan and Ceyhan Rivers northwest of İskenderun Bay. The regional climate is typical of the Eastern Mediterranean, with hot, humid summers and rainy, mild winters, and short transitional seasons. Northerly winds dominate the winter (November to March), and a sea-breeze system with southwesterly winds dominate the summer (April to October). Weather steered by steep mountain ranges but intercepted by valleys along the northern shore, such as at the Göksu river valley and the Gulf of İskenderun, of-

OSD

3, 1481–1514, 2006

ten develops local gale force winds in winter (Reiter 1975; Özsoy, 1981). Eddies and meanders, wind driven currents, topographic/continental shelf waves, inertial/internal oscillations add significant variability to the basic cyclonic circulation exemplified by the satellite SST (Fig. 2a), the bifurcating mid-basin jet and the Asia-Minor current along the Turkish coast, interspersed with quasi-permanent anticyclonic eddies in the Eastern Mediterranean (Wüst, 1961; The POEM Group, 1992; Özsoy et al., 1993). Focusing on the Cilician Basin with the nested model simulations (Fig. 2b) described in the sequel, produces similar features to those observed via satellite. The classical picture of surface circulation in the Gulf of İskenderun after Collins and Banner (1979) aided by satellite imagery and unpublished observations of IMS-METU in the region are schematized in Fig. 2c. Two main types of circulation were observed within the İskenderun Bay: in summer, two counter rotating eddies driven by surface currents entering west of the Bay were inferred, while in winter it was supposed that the currents following the eastern coast could enter east of the Bay. Less saline and cooler waters were observed in the inner part of the Bay. Direct current measurements carried out in winter 1992 indicated several high frequency oscillations in addition to an oscillation of about eight days period with current speeds in the range of 5–25 cm/s. The Cilician Basin coastal system is presently experiencing significant environmental stresses as a result of explosive increases in population, industrial, agricultural and tourism activities. Wastes from industries (steel, paper, fertilizer etc.) and untreated or primary-treated municipal wastes from major towns of Mersin, Adana, İskenderun and Antakya are potential sources of marine pollution. Civilian and military marine transport linked to the harbours of Mersin, İskenderun and Taşucu, oil storage and pipeline terminals at Yumurtalık, Ceyhan and Dörtyol (including the recently completed Baku-Tblisi-Ceyhan pipeline transporting oil and gas from the Caspian Sea) are additional activities with potential impact on the environment. Perennial rivers Göksu, Lamas, Tarsus, Seyhan, Ceyhan and Asi plus some smaller rivers account for a total fresh water flux of 27 km^3/yr (870 m^3/s), accounting for about half the river discharge along the Turkish Mediterranean – Aegean coasts, but much greater than the present dis-

charge of the Nile in the Eastern Mediterranean (estimated to be 540 m^3/s, Pinardi et al., 2005). Following the almost 90% reduction in the discharge of the River Nile in the 1960's, Turkish rivers concentrated in the Cilician Basin presently seem to be the main fresh water and nutrient sources for the entire Levantine Basin of the oligotrophic Eastern Mediterranean. Because of the significant inputs of these rivers, the Cilician Basin has all the characteristics of the ROFI (regions of freshwater influence) but in the oligotrophic environment typical of the Eastern Mediterranean Sea.

2 Cilician Basin/Shelf circulation modeling

The Cilician Basin/Shelf Model domain covers the area shown in Fig. 1, with the horizontal grid characteristics given in Table 1, with a uniform nominal horizontal grid resolution of 1.35 km in both directions, and vertical resolution of 28 sigma levels. The external and internal integration time steps were Δt_e=2 s and Δt_i=40 s respectively, and model constants were: horizontal mixing coefficients A_m=A_h=200 m^2/s, initial vertical mixing coefficients K_m=K_h=K_s=2×10^{-4} m^2/s respectively for momentum, heat, salt and bottom roughness parameters z_0=0.01, $C_{b,min}$=0.0025. The fine scale model bathymetry was generated from contour data of UNESCO bathymetric maps of Mediterranean, making limited use of the US Navy DBDB1 gridded bathymetry to fill areas shallower than 50 m where contour data were missing. The model bathymetry was then filtered with a selective filter that smoothes only the steep slope areas so that the r-value $r=\Delta H/(2H)$ (where H is the depth) between adjacent grid points remains below r=0.2. There were large differences between the coarse grid ALERMO bottom topography and the fine grid Cilician Basin model bottom topography (Fig. 3), which were even larger before the bathymetry data of the former was improved. In general, the Gulf of İskenderun shelf area was deeper in the coarse grid, while the area surrounding the northeastern tip of Cyprus was shallower in the coarse grid. These differences are still significant but were much better for the improved ALERMO bathymetry data.

The bathymetry at about 10 rows of grids at open boundary sections were taken to be exactly the same as the coarse model, regardless of the fine topography created, in order to conserve volume fluxes and transport properties between the coarse and fine grid models, and gradually melded into the interior fine topography.

The interpolation to the fine grid point from the surrounding eight coarse grid data points (or the number of available points) was made by weighted averaging using the following weights at each of the eight coarse grid points:

$$W_k(x,y,z) = \exp -[(x_c - x_f)^2 + (y_c - y_f)^2 / s_h^2] . \exp -[(z_c - z_f)^2 / s_v^2], k = 1,8$$

where s_h and s_v are scales for horizontal and vertical influences respectively and x, y, z are coordinates with subscript c indicating the coarse and f indicating the fine grid points. Because both the coarse and fine grid coordinates are originally in sigma coordinates, the vertical scale s_v was locally adjusted to be representative of the average vertical distance between the coarse grid points, so that more uniform weighting was obtained in the shallow area as compared to the deep area. Because the coarse grid widely differs from the fine grid, especially near the bottom and the coast, special care was taken for interpolation near these areas. The few coastal points outside the coarse domain were extrapolated from data at the same depth. The deep data outside the coarse domain were interpolated from the data above its depth using the above 8 point scheme but including only those points where there were data available. The effect of this scheme is to replace data points with values available in the upper layers, and seemed to be performing well considering the rather uniform properties at great depth. The bottom values from the coarse model (the last vertical grid point) were values not used by the model, and therefore eliminated from the interpolation. Data availability near the bottom was an issue that strongly affected interpolation, because the coarse grid domain was often shallower than the fine grid domain in shelf regions. At intermediate depths this is not a very severe problem, because data are only missing in limited areas such as near the coasts and the vicinity of the sharp northeast Cape of Cyprus. At the bottom layer of the fine grid the number of data available for interpolation from the lower layer decreases greatly, due to the shallower limits of the

coarse domain in same areas. The data in those areas were filled mostly by interpolation from the data available in the upper layer. Open boundary conditions tested for nested domains in the Mediterranean Forecasting System MFS (e.g. papers in De Mey et al., 2003 special volume for MFS), namely the specification of barotropic flow velocity with a radiation component on the normal component (Flather b.c.), baroclinic velocity components and temperature/salinity with advective conditions during outflow have been adopted in the present model. Instantaneous momentum, heat and salt flux boundary conditions at the sea surface,

$$K_m(du/dz) = T_x,$$

$$K_m(dv/dz) = T_y,$$

$$c_p K_h(dT/dz) = Q_h$$

$$K_s(dS/dz)=S(E-P)$$

are specified for wind stress components T_x, T_y, net heat flux Q_h and salt flux $Q_s=S(E-P)$ with surface salinity S and net water flux at the surface (evaporation minus precipitation $E-P$), where the fluxes are specified through either an atmospheric boundary layer formulation or bulk formulae. Sensitivity to surface fluxes was tested making runs with identical initial and lateral but with alternative surface boundary conditions for the January 2003 validaton period (in all cases ALERMO open boundary and initial conditions were used): Run A: non-interactive surface heat and salt fluxes are are iteratively computed by the atmospheric boundary layer formulation following Launiainen and Vihma (1990), Vihma (1995), and Ibrayev et al. (2004)[1], based on the Monin-Obukhov similarity theory, making use of the atmospheric surface variables, SST and long wave and short wave radiation data provided by the SKIRON atmospheric model. The 2 m dew point temperature and 10 m winds are used to compute

[1] Ibrayev, R. A., Özsoy, E., Schrum, C., and Sur, H. İ.: Sur Seasonal Variability of the Caspian Sea – Three-Dimensional Circulation and Air-Sea Interaction, unpublished, 2004.

variables and fluxes at 10 m height within the iterative scheme. Run B: surface heat and salt fluxes interactively calculated by the by the atmospheric boundary layer formulation as in Run A, using the SKIRON surface atmospheric variables and model generated SST. Run C: surface heat and salt fluxes including short and long wave radiation calculated by bulk formulae after Bignami et al. (1995); Castellari et al. (1998); Korres and Lascaratos (2003), using SKIRON surface atmospheric variables and model generated SST. The model is apparently based on a combination of the Bignami et al. (1995) long wave radiation fluxes and Kondo (1975) sensible and latent heat fluxes, with the short wave radiation fluxes specified according to Rosati and Miyakoda (1988). The method employs the 10 m winds together with 2 m dew point temperature data as they are provided by the ETA model. Run D: Same as Run B except for penetrative radiation has been used. Temperatures at 10 m after a one month run with continuous forcing in January 2003, compared in Fig. 4 for the above cases, show differences between the tested cases, but at this point it is not possible to objectively assess which one should be better. The case A with non-interactive fluxes indicates much faster cooling of surface waters as compared to the other cases. The interactive flux computations of case B and the flux computations using bulk formulae in case C do not seem to produce very different rates of cooling, but there are significant differences in the resulting surface circulation. The penetrative radiation case D results in much lower rates of cooling. Other comparisons between fields show significant changes especially up to a depth of 100 m. The different mixing characteristics produced by the flux specifications in cases A–D are compared in the salinity sections of Fig. 5. The low salinity modified Atlantic water present at mid-depths is used as a tracer to show differences in mixing, as they are influenced by the surface momentum, heat and salt fluxes. Finally the comparison of surface fluxes for the above cases during the January 2003 period is provided in Fig. 6. It is evident that the fluxes of all interactive computation cases B, C, D are similar to each other, but very different from the non-interactive case A which uses constant surface salinity and surface variables provided from the atmospheric model. In particular, the salt flux for the non-interactive is not realistic because

of the constant surface salinity value assigned, and the heat fluxes are much higher than the other cases. On the other hand, the flux computations using the bulk formulae in case C, produce slightly higher salt and lower heat fluxes from the sea surface to the atmosphere, in comparison to the atmospheric boundary layer formulation in cases B and D. The non-penetrative versus penetrative radiation formulation in cases B and D of course do not affect the fluxes, but the latter results in lower rate of cooling as a result of the radiation heat source distributed near the surface waters.

3 Operational forecasts

An intensive data collection and assimilation effort was made during the 6 month Target Operational Period beginning in September 2004, producing weekly forecasts of 5 days for the entire series of nested MFSTEP model domains. Examples of forecasts are provided here. In September–November 2004 period, the persistent anticyclonic eddy east of Cyprus (Figs. 2a, b) moved north (Fig. 7a) and created persistent jet flows (Fig. 7b) following the "tip" of Cyprus, impinging on the Gulf of İskenderun, and feeding the Asia Minor current flowing west along the northern continental slope. In mid-November a sudden change in direction of surface currents due to wind and remote forcing (Fig. 7c) was followed by a temporary switch in currents in December and January to flow along the Syrian coast (Figs. 7d, e). The flow through the Cilician Basin was observed to have a significant barotropic component with current speeds reaching up to 0.3 m/s at 500 m depth. In June 2005 an upwelling event developed simultaneously south of Cyprus and along the Turkish coast in western Cilician Basin (Fig. 7f), which was well reproduced in the model (Fig. 7g). Shelf scale motions are displayed by focusing into specific regions. The meso-scale circulations developed in İskenderun Bay are exemplified in Fig. 7h. In this example, the flow along the shelf slope bypasses the Bay across its southwest opening, while a branch circulates cyclonically in the Bay, as suggested earlier in Fig. 2c. Other types of circulation entering the bay on the surface with a return flow at deeper layers were also detected. However unsteady

effects resulting from weekly initialization cycles affected the results, and were recently remedied by continuous forecasts that were implemented.

4 Evaluating extended forecasts

The performance of the model forecasts in active and slave mode, i.e. the model initialized and running with continuously updated surface and lateral boundary conditions compared with the model re-initialized at intervals was evaluated. For this purpose the January 2005 data were used to make forecasts for a full month with continuous updates versus the model re-initialized every week. The comparison of the circulations at the target date of 27 January 2005 for forecasts re-initialized at weekly intervals are given in Figs. 8 and 9 for depths of 10 m and 800 m respectively. At 10 m the forecasts (Fig. 8) at the target date do not differ too much for the initializations done 3–4 weeks before the target date, but seem to deteriorate in features for initializations 1–2 weeks before the target date. At 800 m depth (Fig. 9), again we see the same result, indicating that at least three-four weeks are needed for the deep features to develop, such as the eddies developed near the bottom as a result of the channel topography of the Cilician Basin. The mean and standard deviations of fields generated from the weekly initializations are compared in Figs. 10 and 11 for depths of 10 m and 100 m respectively. It is clearly indicated that the weekly forecasts can not build up the kinetic energy compared to longer forecasts. The temperature and salinity fields show similar mean values but with very different details indicated by the standard deviations. The salinity change appears the same as in the coarse model, while the temperature initial conditions from the coarse model at weekly intervals are different from those forecasted by the fine scale model because of different flux formulations and resolution.

5 Conclusions

Experience and development achieved during the MFSTEP exercise give sufficient confidence for forecasting Cilician Basin circulation at high resolution shelf scales. The extension of the model domain to the entire northern Levantine coast and shelf regions along Asia Minor are under way.

Acknowledgements. This work was supported by the MFSTEP project (contract no EVK-CT-2002-00075, 2003-2006) under FP5 of the Commission of the European Community, with N. Pinardi as the coordinator. We thank Ş. Beşiktepe and the Institute of Marine Sciences of METU for support, and H. Örek for the satellite data processing. Related studies currently are being continued under the Cilician Basin (TÜBITAK 105Y277) and MOMA (TÜBITAK 105G029) projects of the Turkish Scientific and Technical Research Council.

References

Bignami, F., Marullo, S., Santoleri, R., and Schiano, M. E.: Longwave Radiation Budget in the Mediterranean Sea, J. Geophys. Res., 100(C2), 2501–2514, 1995.

Castellari, S., Pinardi, N., and Leaman, K.: A Model Study of Air-Sea Interactions in the Mediterranean Sea, J. Mar. Syst., 18, 89–114, 1998.

Collins, M. B. and Banner, F. T.: Secchi disk depths, suspensions and circulation in Northeastern Mediterranean Sea, Marine Geology, 31, M39–M46, 1979.

De Mey, P., Lascaratos, A., Manzella, G., and Pinardi, N. (Guest Editors): Mediterranean Forecasting System Pilot Project – Parts I and II, Ann. Geophys. (Special Issue), 21, 436, 2003.

Horton, C., Clifford, M., Schmitz, J., and Kantha, L. H.: A real-time oceanographic nowcast/forecast system for the Mediterranean Sea, J. Geophys. Res., 102(C11), 25 123–25 156, 1997.

Kondo, J.: Air-sea bulk transfer coefficients in diabatic conditions, Boundary-Layer Meteorol., 9, 91–112, 1975.

Korres, G. and Lascaratos, A.: A one-way nested eddy resolving model of the Aegean and Levantine basins: Implementation and Climatological Runs, Ann. Geophys., 21, 205–220, 2003.

Launiainen, J. and Vihma, T.: Derivation of turbulent surface fluxes – an iterative flux-profile method allowing arbitrary observing heights, Environmental Software, 5(3), 113–124, 1990.

Özsoy, E.: On the Atmospheric Factors Affecting the Levantine Sea, European Center for Medium Range Weather Forecasts, Reading, UK, Technical Report No. 25, 30p, 1981.

Özsoy, E., Hecht, A., Ünlüata, Ü., Brenner, S., Sur, H. İ., Bishop, J., Latif, M. A., Rozentraub, Z., and Ouz, T.: A Synthesis of the Levantine Basin Circulation and Hydrography, 1985–1990, Deep-Sea Res., 40, 1075–1119, 1993.

Pinardi, N., Arneri, E., Crise, A., Ravaioli, M., and Zavatarelli, M.: The physical, sedimentary and ecological structure and variability of shelf areas in the Mediterranean Sea, The Sea, 14, 2005.

Reiter, E. R.: Handbook for Forecasters in the Mediterranean, Weather Phenomena of the Mediterranean Basin, Part 1: General Description of the Meteorological Processes, Tech. Pap. 5–75, 344 pp., Environmental Prediction Research Facility, Naval Postgraduate School, Monterey, California, 1979.

Rosati, A. and Miyakoda, K.: A general circulation model for upper ocean simulation, J. Phys.

Oceanogr., 18(11), 1601–1626, 1988.
The POEM Group: Robinson, A. R., Malanotte-Rizzoli, P., Hecht, A., Michelato, A., Roether, W., Theocharis, A., Ünlüata, Ü., Pinardi, N., Artegiani, A., Bishop, J., Brenner, S., Christianidis, S., Gacic, M., Georgopoulos, D., Golnaraghi, M., Hausmann, M., Junghaus, H.-G., Lascaratos, A., Latif, M. A., Leslie, W. G., Oğuz, T., Özsoy, E., Papageorgiou, E., Paschini, E., Rosentroub, Z., Sansone, E., Scarazzato, P., Schlitzer, R., Spezie, G.-C., Zodiatis, G., Athanassiadou, L., Gerges, M., and Osman, M.: General Circulation of the Eastern Mediterranean, Earth Sci. Rev., 32, 285–309, 1992.
Vihma, T.: Atmosphere-Surface Interactions over Polar Oceans and Heteregenous Surfaces, Finnish Marine Research, 264, 3–41, 1995.

Table 1. Domain and grid characteristics of the Cilician Basin / Shelf Model n.m – dimensions of grid, λ. ϕ – longitude and latitude coordinates. x. y – distance coordinates.

n	$\Delta\lambda$ (°)	Δx (km)	λ_1 (°)	λ_2 (°)	λ_2–λ_1 (°)	x_2–x_1 (km)
303	0.01500	1.35	31.700	36.245	4.545	408.6
m	$\Delta\phi$ (°)	Δy (km)	ϕ_1 (°)	ϕ_2 (°)	ϕ_2–ϕ_1 (°)	y_2– y_1 (km)
150	0.01206	1.35	35.120	36.929	1.809	201.1

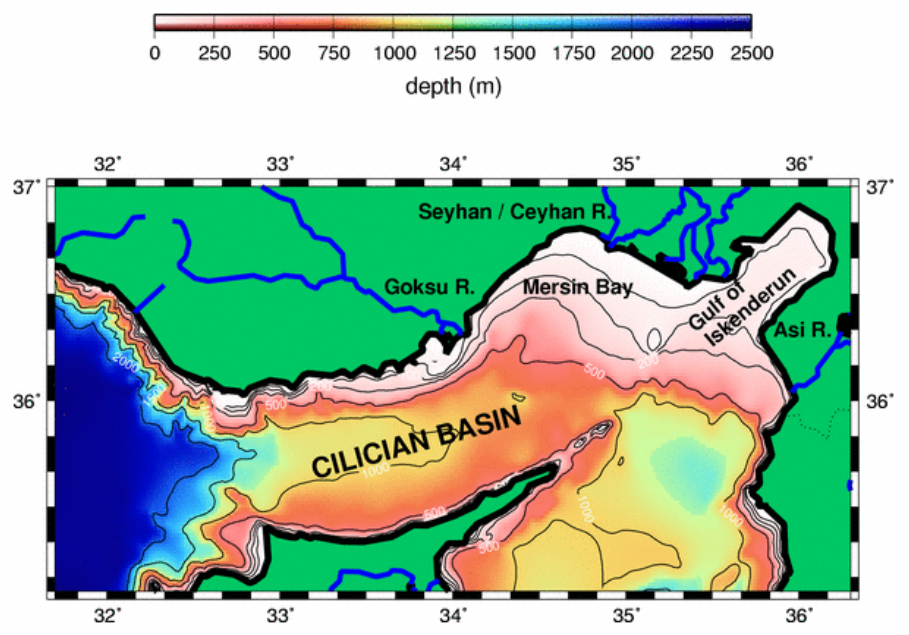

Fig. 1. Layout of the Cilician Basin showing the topography, important rivers and bays.

OSD
3, 1481–1514, 2006

E. Özsoy and A. Sözer

EGU

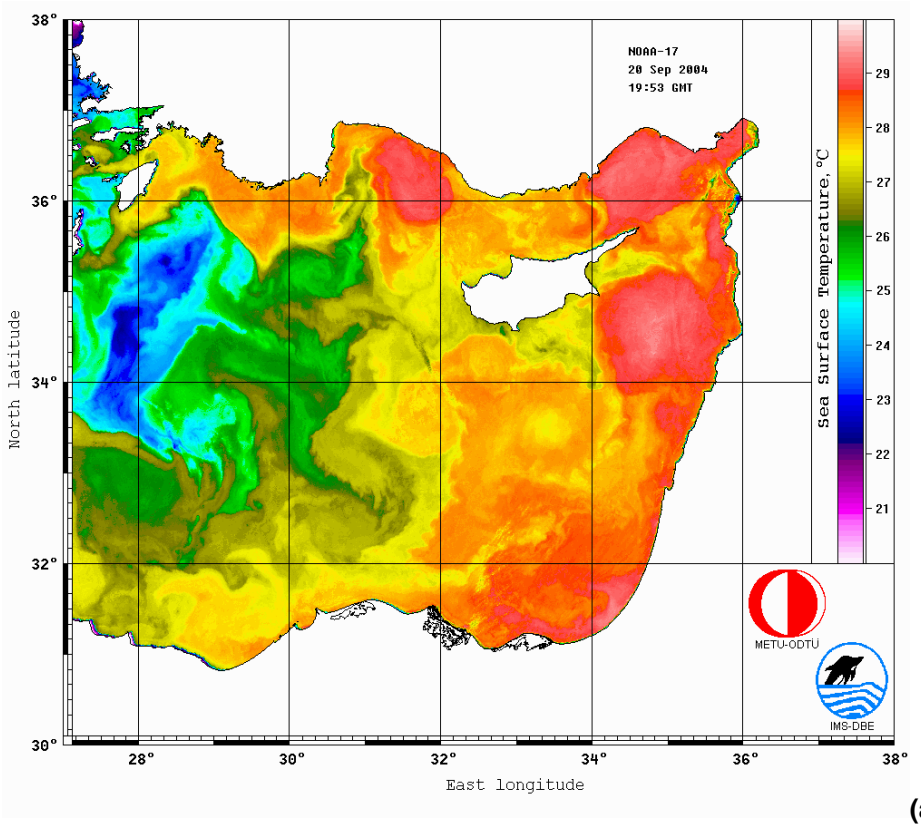

Fig. 2. **(a)** Eddies, jets and gyres in the Levantine Basin of the Eastern Mediterranean Sea revealed in satellite-derived sea surface temperature field of 28 September 2004, **(b)** Cilician Basin model 5 day forecast of 10 m currents and temperature on 27 September 2004, **(c)** schematic surface circulation of Mersin Bay and the Gulf of İskenderun area (continuous line: summer, dashed line: winter) suggested by Collins and Banner (1979).

OSD
3, 1481–1514, 2006

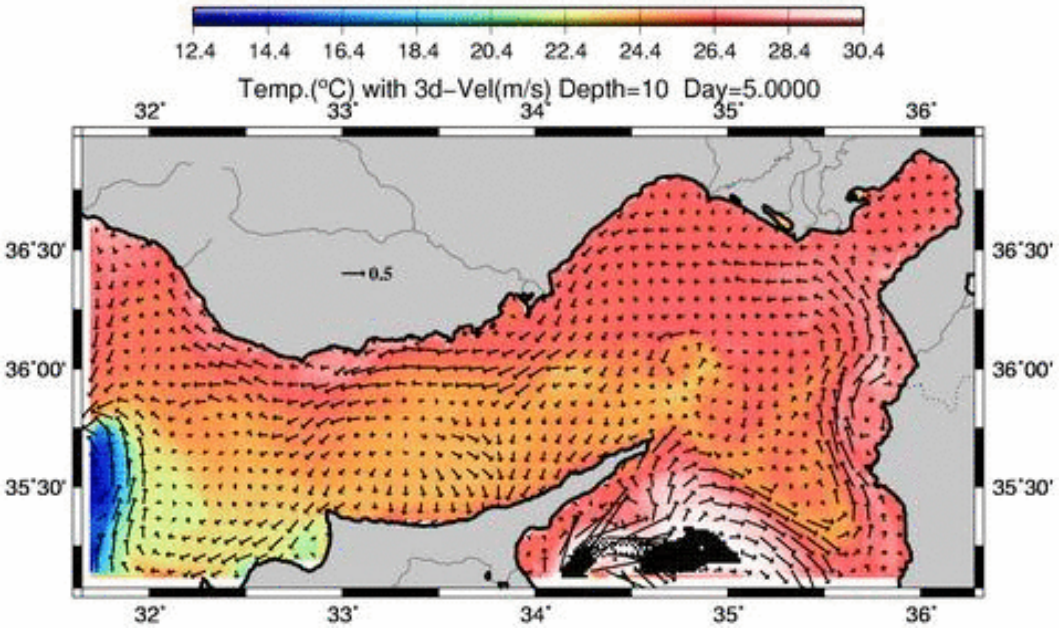

(b)

Fig. 2. Continued.

OSD
3, 1481–1514, 2006

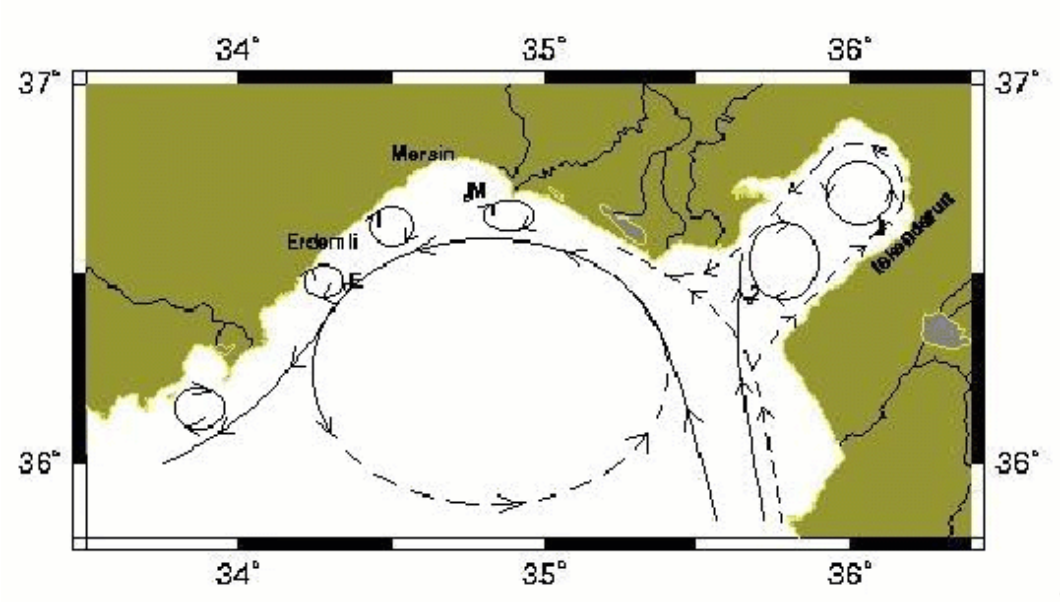

(c)

Fig. 2. Continued.

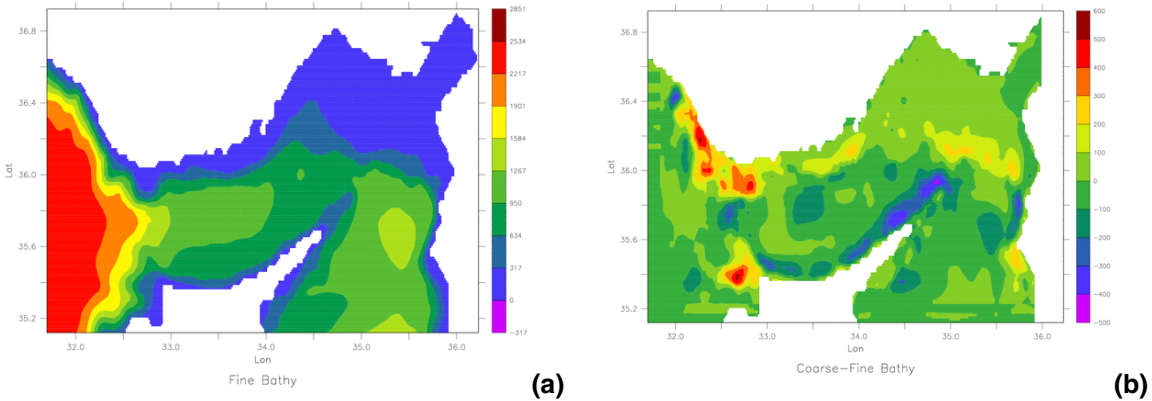

Fig. 3. Model bathymetry (depth in m) of **(a)** the fine grid Cilician Basin/Shelf Model, and **(b)** the difference between coarse and fine grid bathymetry data sets with coarse grid data interpolated and the difference calculated on the fine grid.

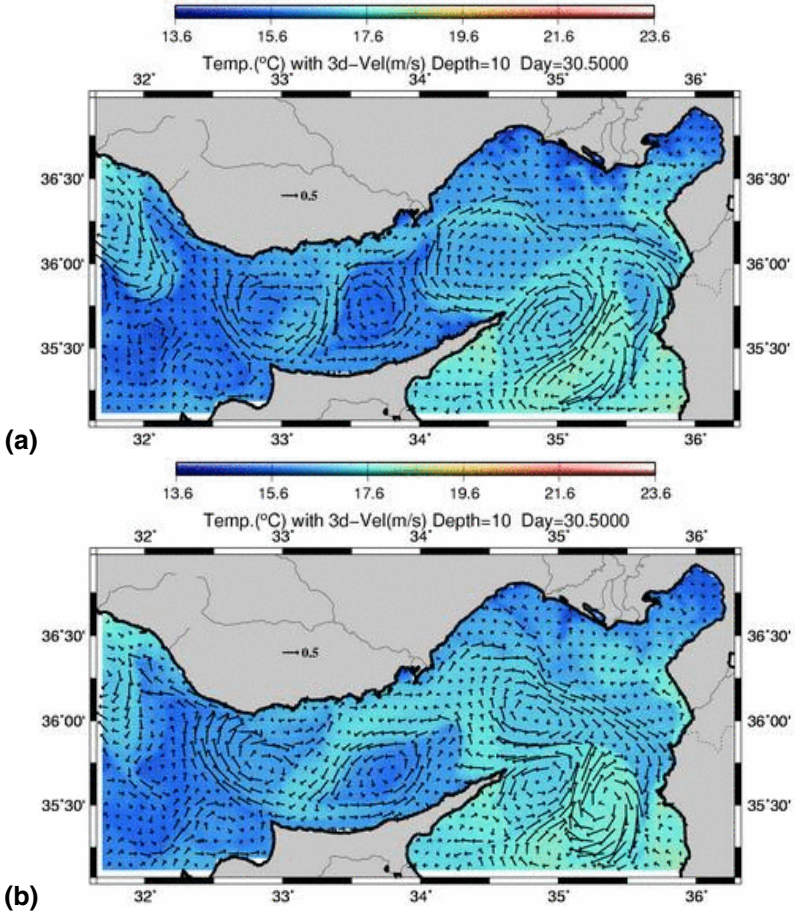

Fig. 4. (a) Currents and temperature at 10 m depth for run A, run B **(b)**, run C **(c)**, run D **(d)** on 31 January 2003 after a one-month run.

OSD
3, 1481–1514, 2006

EGU

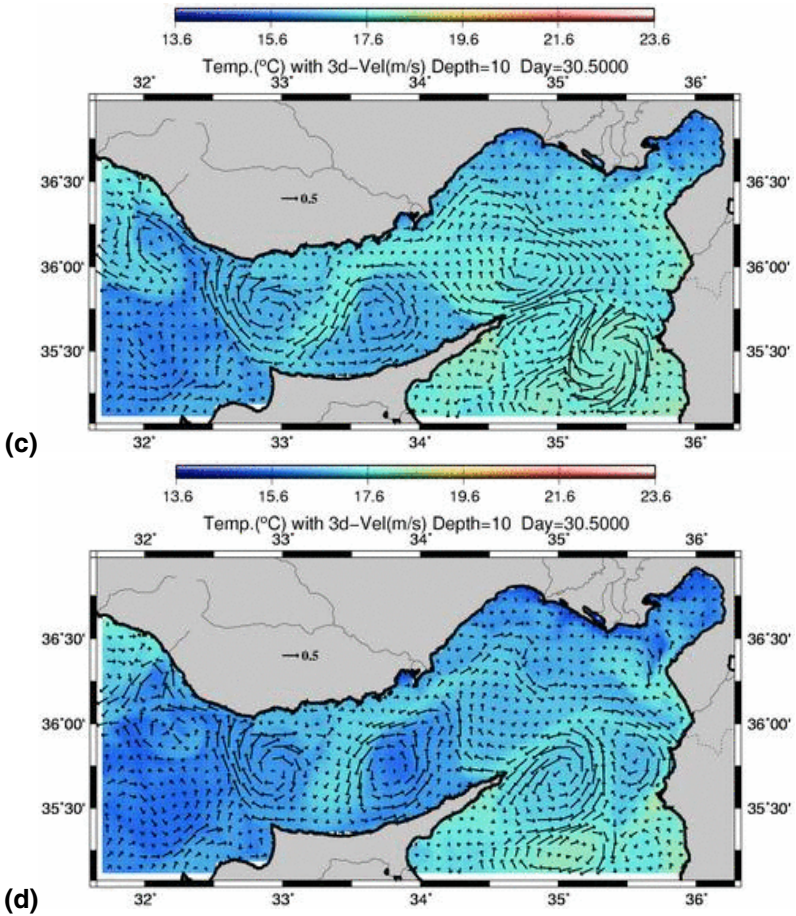

Fig. 4. Continued.

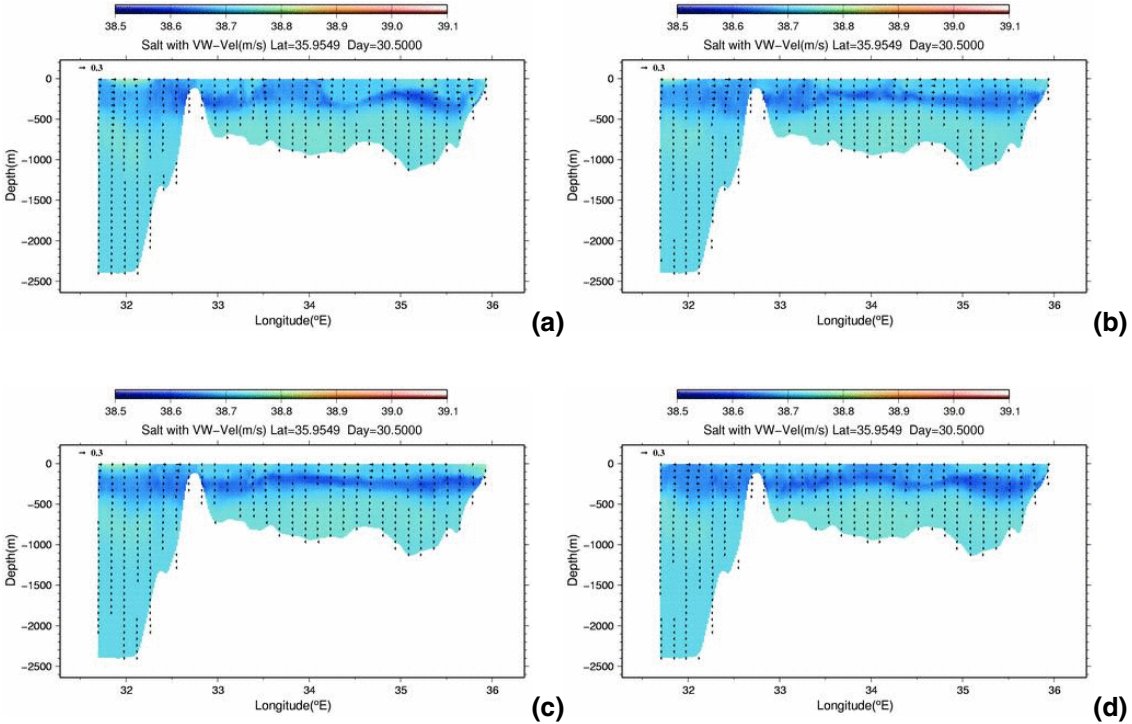

Fig. 5. Comparison of salinity fields along the west-east section at 36° N for **(a)** run A, **(b)** run B, **(c)** run C, **(d)** run D, on 31 January 2003 after a one-month run.

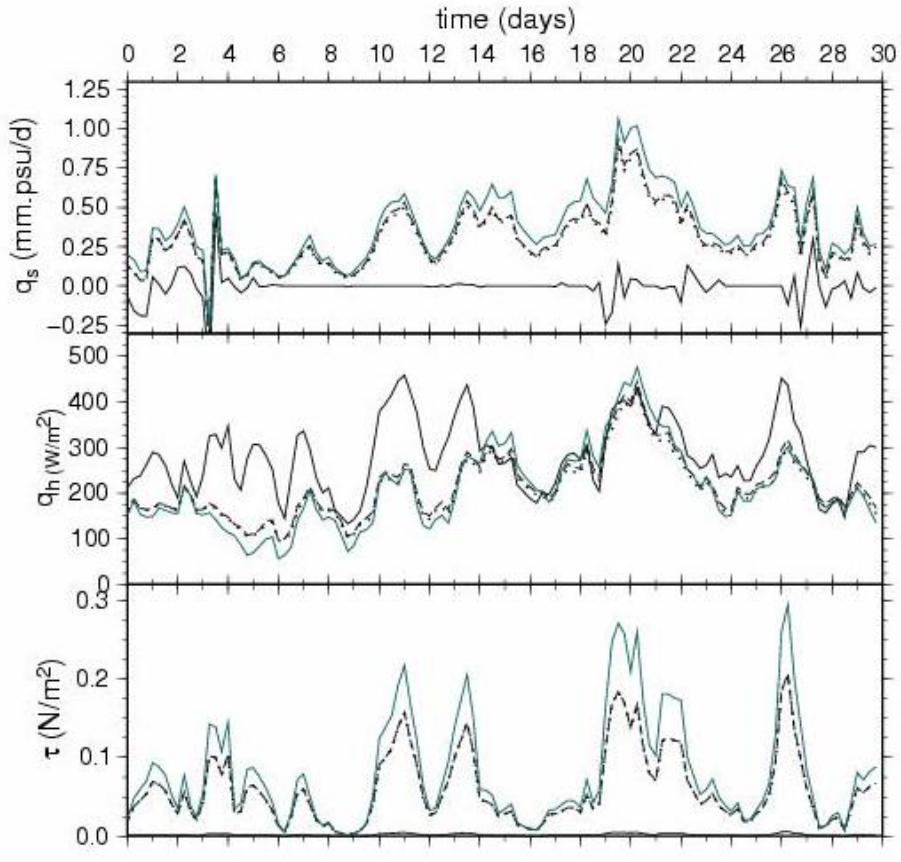

Fig. 6. **(a)** Salt flux, **(b)** heat flux and **(c)** wind stress for runs A (solid line), B (dashed line), C (dotted line) and D (solid line in light colour) during January 2003.

OSD
3, 1481–1514, 2006

EGU

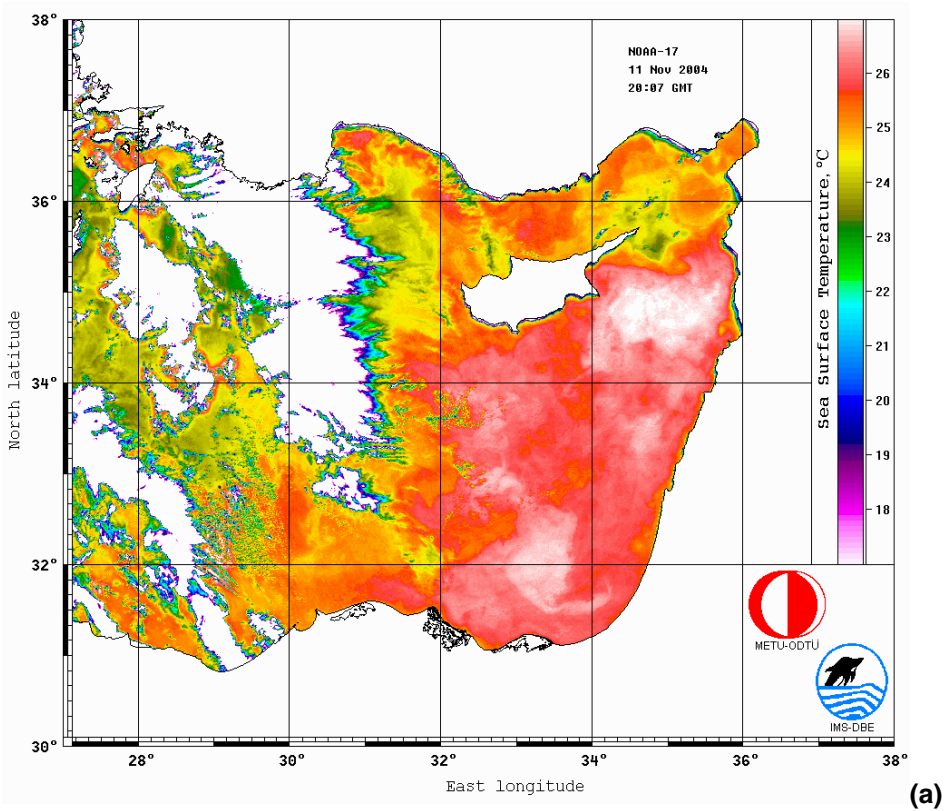

Fig. 7. **(a)** Satellite sst image on 11 November 2004, **(b)** forecast currents and temperature at 10 m depth for a 5 day forecast on 8 November 2004, 12:00 UTC **(c)** same for 22 November 2004 and **(d)** 6 December 2004, **(e)** sst image on 11 January 2005 **(f)** sst image on 17 June 2005, **(g)** currents and temperature at 10 m depth for 21 June 2005, **(h)** currents and temperature at 5 m depth in İskenderun Bay on 13 September 2005.

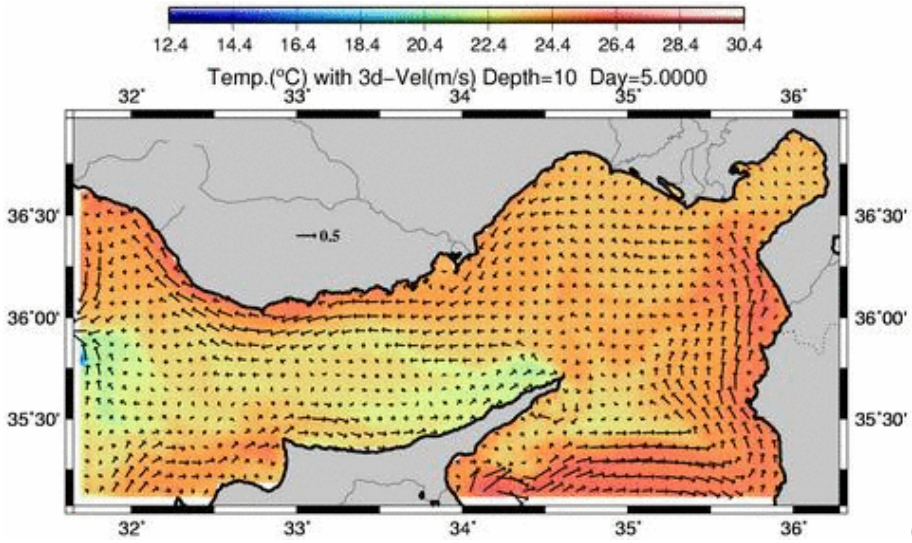

(b)

Fig. 7. Continued.

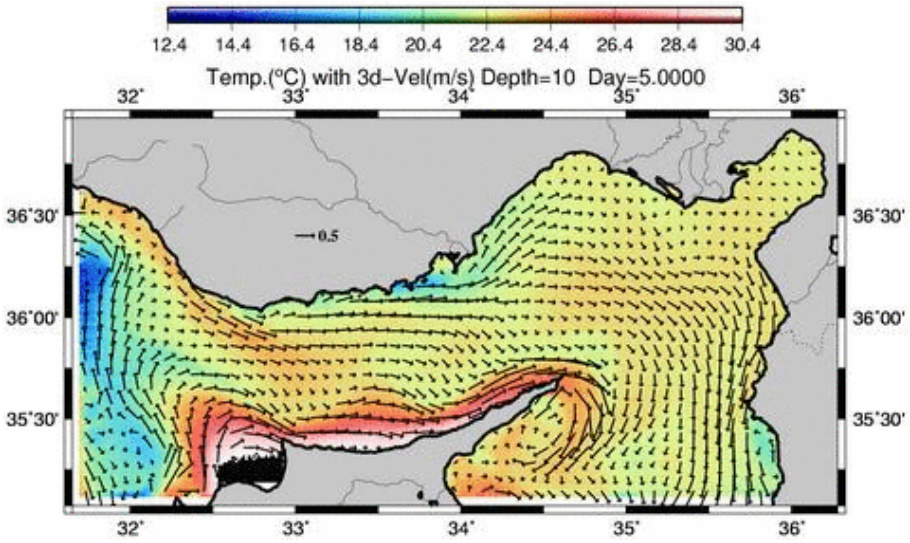

(c)

Fig. 7. Continued.

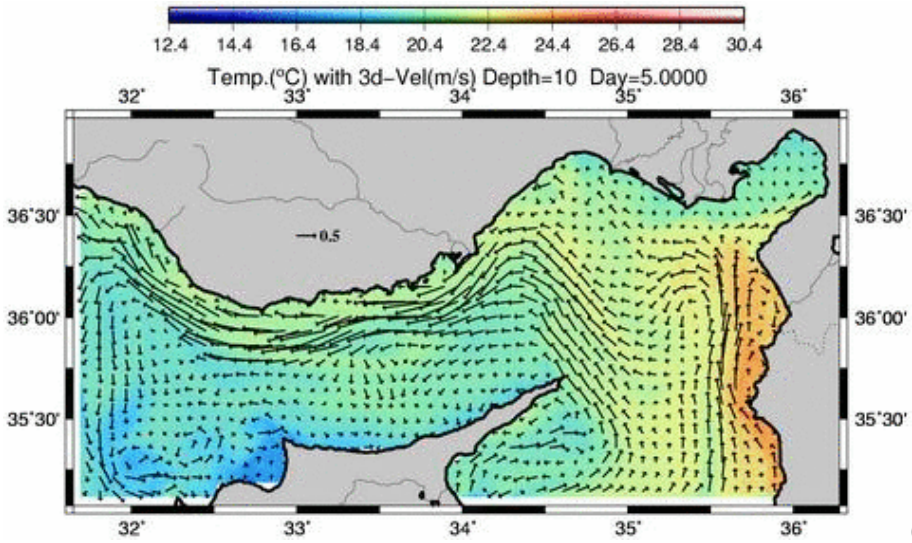

(d)

Fig. 7. Continued.

OSD
3, 1481–1514, 2006

EGU

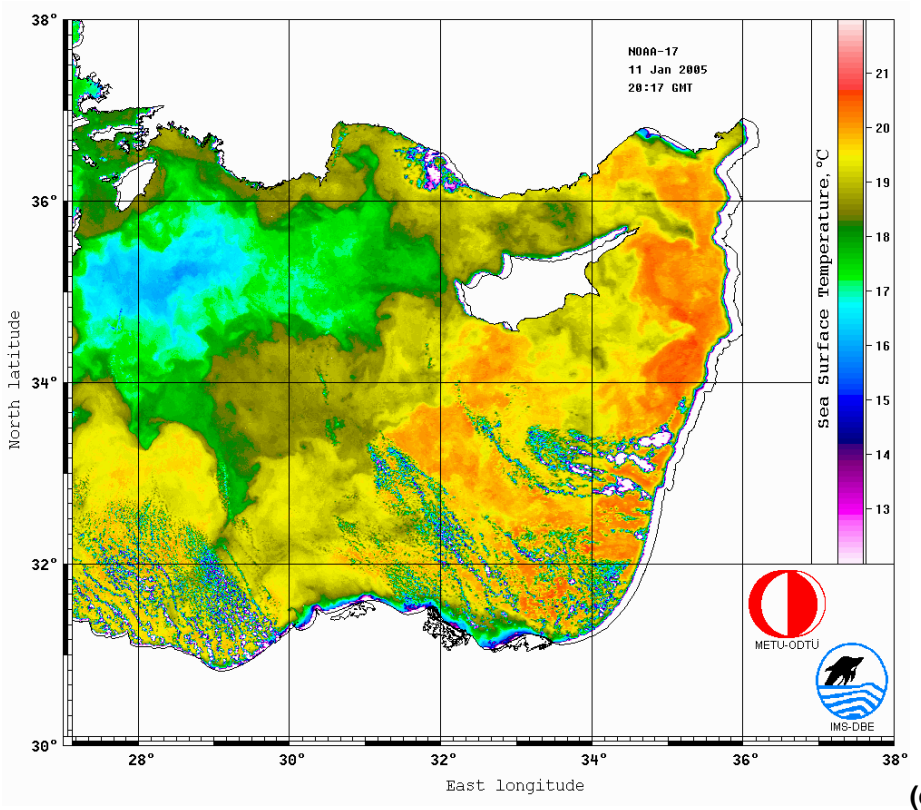

(e)

Fig. 7. Continued.

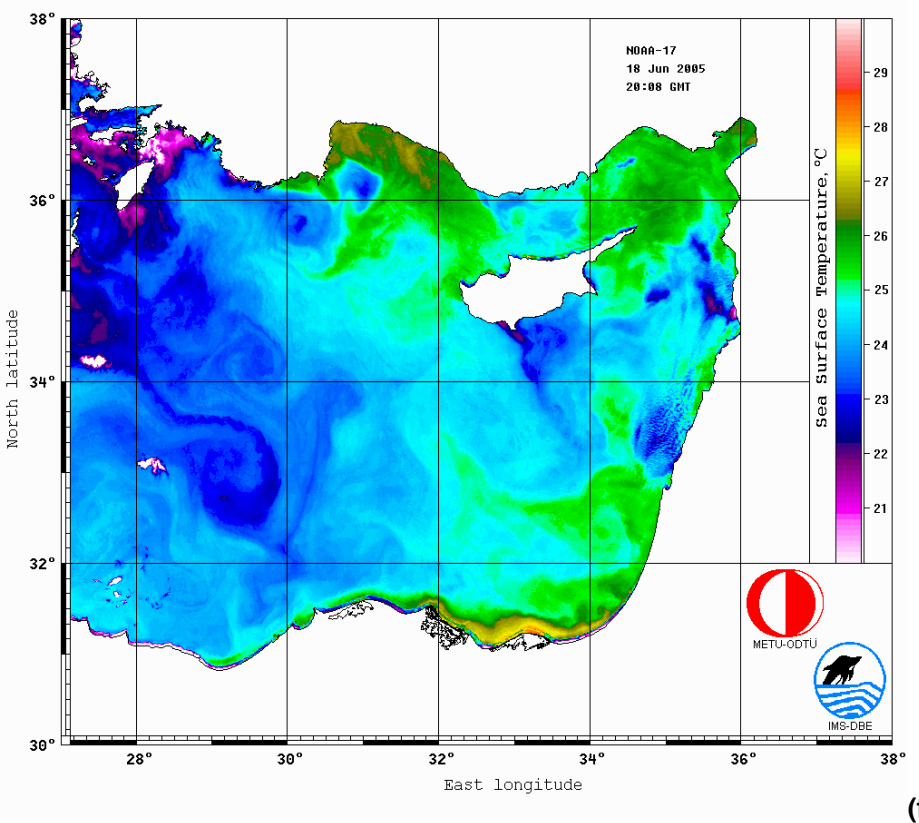

(f)

Fig. 7. Continued.

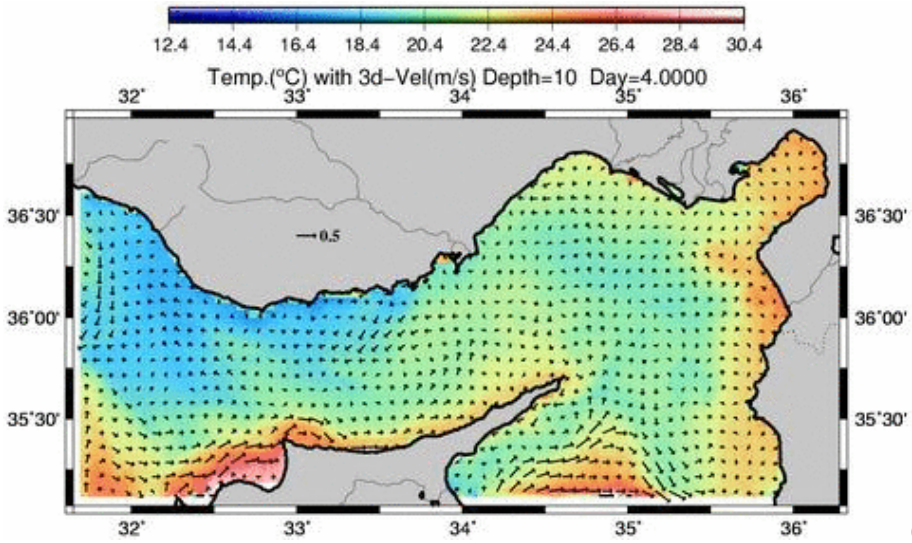

(g)

Fig. 7. Continued.

OSD
3, 1481–1514, 2006

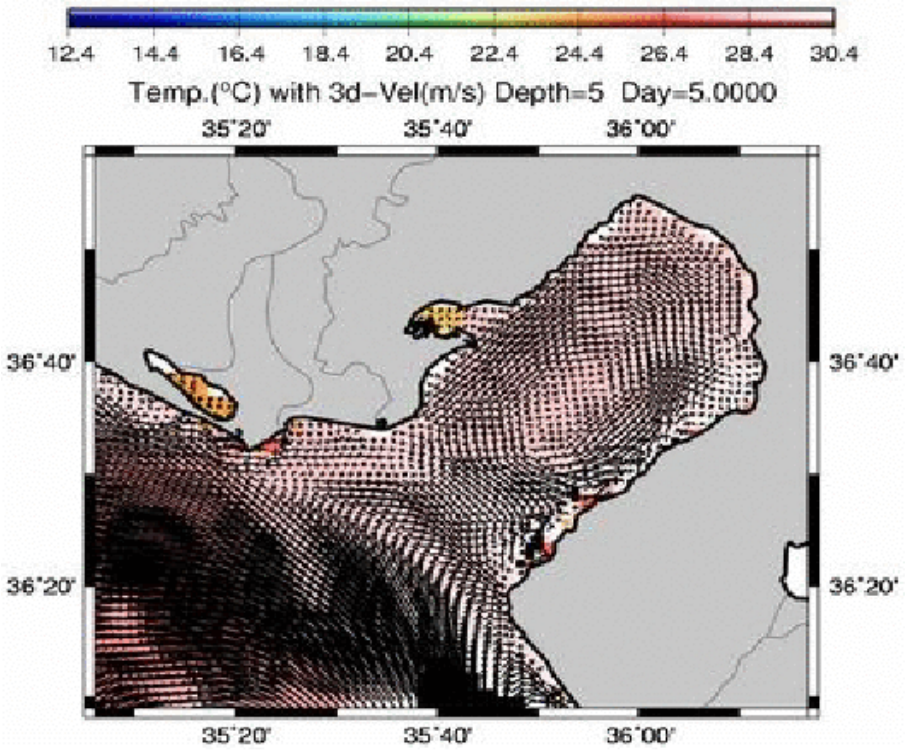

Fig. 7. Continued.

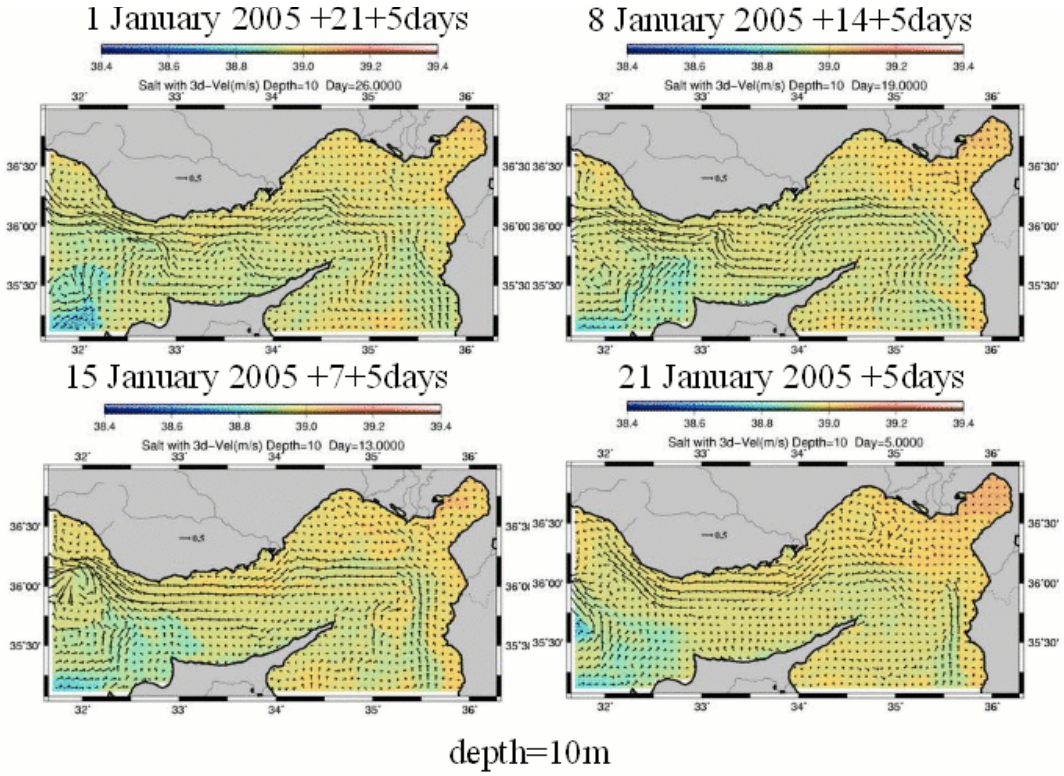

Fig. 8. Comparison of forecasts at 10 m depth at the target date of 27 January 2005 for runs initialized at different dates and run with continuously updated hourly atmospheric fluxes and daily lateral boundary conditions through January 2005. Initializations are on **(a)** 1 January, **(b)** 8 January, **(c)** 15 January and **(d)** 22 January 2005.

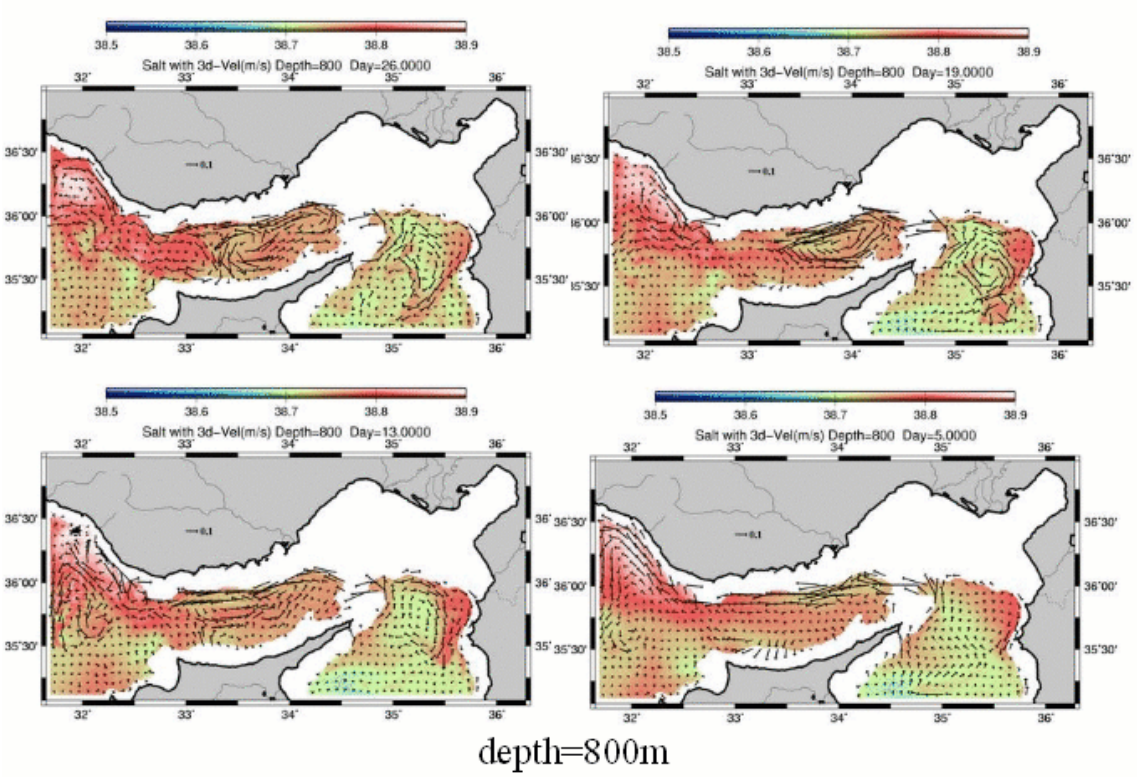

Fig. 9. Comparison of forecasts at 800 m depth at the target date of 27 January 2005 for runs initialized at different dates and run with continuously updated hourly atmospheric fluxes and daily lateral boundary conditions through January 2005. Initializations are on **(a)** 1 January, **(b)** 8 January, **(c)** 15 January and **(d)** 22 January 2005.

OSD
3, 1481–1514, 2006

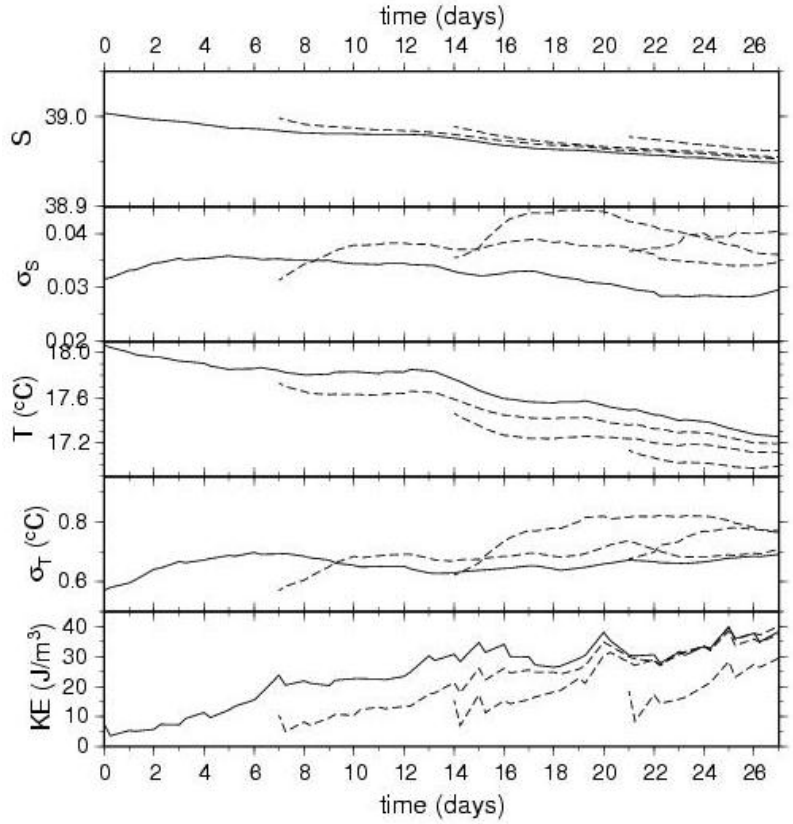

Fig. 10. Comparison of runs initialized at different dates and run with continuously updated hourly atmospheric fluxes and daily lateral boundary conditions through January 2005. Comparison of field statistics averaged over the model domain at 10 m depth **(a)** mean salinity, **(b)** standard deviation of salinity **(c)** mean temperature **(d)** standard deviation of temperature **(e)** kinetic energy density. Initializations are on 1 January 2005 (solid line), 8 January, 15 January and 22 January (dashed lines) 2005.

OSD
3, 1481–1514, 2006

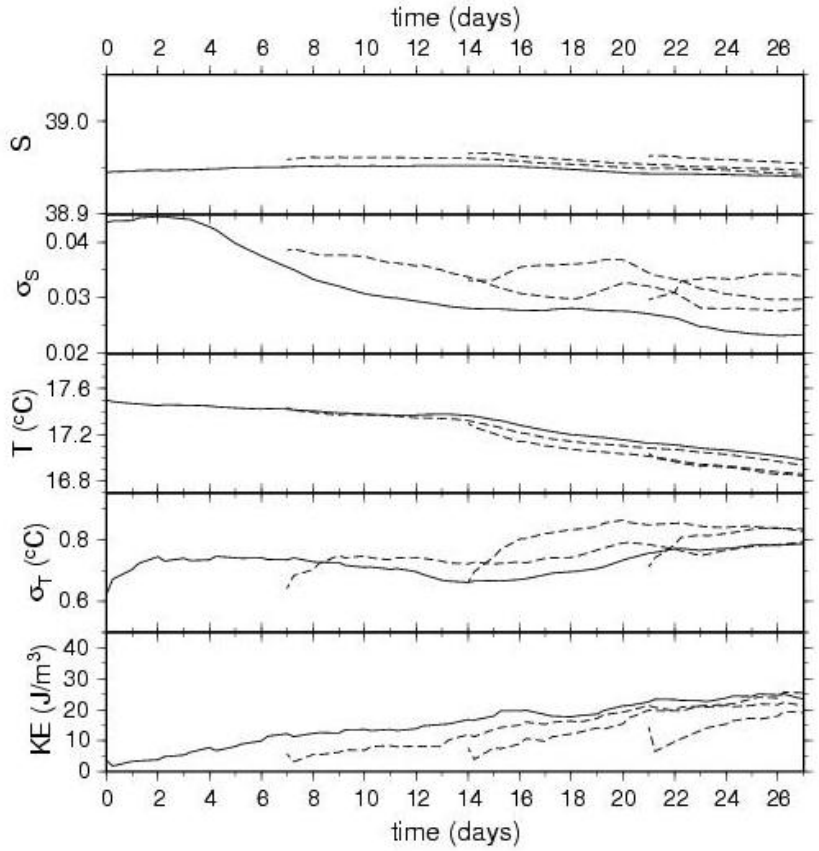

Fig. 11. Comparison of runs initialized at different dates and run with continuously updated hourly atmospheric fluxes and daily lateral boundary conditions through January 2005. Comparison of field statistics averaged over the model domain at 100 m depth **(a)** mean salinity, **(b)** standard deviation of salinity **(c)** mean temperature **(d)** standard deviation of temperature **(e)** kinetic energy density. Initializations are on 1 January 2005 (solid line), 8 January, 15 January, and 22 January (dashed lines) 2005.

OSD
3, 1481–1514, 2006